Deep learning-driven multi-omics integration reveals potential ferroptosis-associated mechanisms of Chinese herbal medicines in colorectal cancer

Tingting Hao
Yunnan Agricultural University
Ya Ning
Yunnan Agricultural University
Mengli Zhang
Guangxi Medicinal Botanical Garden
qiao zhu
Guangxi Medicinal Botanical Garden
dawei li
Yunnan Agricultural University
die jiang
Yunnan Agricultural University
yanqi liu
Yunnan Agricultural University
Xingzhi Yang
Kunming Institute of Botany
Xing Jiang
Guangxi Medicinal Botanical Garden
Xiaolei zhou
Guangxi Medicinal Botanical Garden
dandan mo
Guangxi Medicinal Botanical Garden
min ou
Guangxi Medicinal Botanical Garden
xuzhen li
Yunnan Agricultural University
qinghua kong
Kunming Institute of Botany
qiangqiang zhu
Yunnan Agricultural University
xiang hua xia
Guangxi Medicinal Botanical Garden
yang dong
loyalyang@163.com
Yunnan Agricultural University
xiaonan yang
Guangxi Medicinal Botanical Garden

weibing wang
Yunnan Agricultural University

Article

Keywords: Deep learning, Multi-omics integration, Chinese herbal medicines, Colorectal cancer, Ferroptosis

Posted Date: August 28th, 2026

DOI: https://doi.org/10.21203/rs.3.rs-10470359/v1

Additional Declarations: No competing interests reported.

Abstract

Chemoresistance and metastasis remain major challenges in colorectal cancer (CRC) treatment. Chinese herbal medicines (CHMs) represent a valuable source of multi-target therapeutic candidates; however, systematic approaches for identifying their potential anti-CRC effects and molecular mechanisms are limited. In this study, we developed an AI-assisted multi-omics framework to screen 187 CHM extracts and investigate their potential regulatory effects in CRC. Transcriptomic profiling combined with deep learning approaches, including Jaccard similarity analysis, autoencoder-based feature learning, multi-kernel learning, and weighted gene co-expression network analysis, was applied for candidate prioritization. Integrated transcriptomic and proteomic analyses were further performed to characterize the associated molecular pathways. Five CHMs were identified as potential candidates associated with ferroptosis regulation and metabolic remodeling in CRC, including *Pinus massoniana* Lamb., *Mahonia fortunei*, and *Coptis chinensis* Franch. These candidates were associated with alterations in iron homeostasis, lipid peroxidation-related processes, IL-6/STAT3 signaling, and cholesterol metabolism pathways. Collectively, this study establishes an AI-driven multi-omics strategy for systematic discovery of CHM candidates and provides insights into their potential roles in regulating ferroptosis-associated and metabolic pathways in CRC.

1. Introduction

Colorectal cancer (CRC) is the third most frequent cancer globally, with more than 1.9 million new cases recorded in 2023. Both its death rate and incidence are increasing(1). Multidrug resistance (MDR) causes therapy failure in about 50% of patients with metastatic colorectal cancer (mCRC), creating a major barrier to available therapeutic choices(2). Effective treatment plans for RAS/RAF-mutant subtypes are still elusive, despite minimal clinical success with molecularly targeted biologics targeting EGFR and VEGF(3). Moreover, inadequate response rates (< 15%) to PD-1/PD-L1 checkpoint inhibitors are caused by immunosuppressive cell infiltration inside the tumor microenvironment (TME), which promotes immune evasion(4). The inflammation-metastasis cascade promotes metastatic niche development via NF-κB/STAT3-TWIST1-mediated epithelial-mesenchymal transition (EMT)(5). Metabolic reprogramming-induced adaptive energy stress reduces intracellular chemotherapeutic drug accumulation(6), and gut microbiota-immune axis dysbiosis perpetuates chronic inflammatory TME via TLR4/MyD88 pathway hyperactivation(7).

Chinese herbal medicines (CHMs) have emerged as a critical resource for anti-CRC drug development owing to their multi-pharmacological synergism and minimal off-target toxicity characteristics(3, 8)According to high-throughput multi-omics platforms including as transcriptomics, proteomics, and metabolomics, phytochemical components demonstrate multidimensional anticancer effectiveness by simultaneously modulating several signaling nodes(9). Bioactive phytocompounds have been shown through systematic pharmacological investigations to target the inflammation-metastasis signaling axis, inhibiting NF-κB/STAT3-TWIST1-driven EMT inside the TME (10), while simultaneously altering gut microbiota-immune-metabolic networks (9). Tanshinone A, for example, reduces inflammation and related tumor progression by inhibiting COX-2 expression, which in turn prevents CRC formation (11). Additionally, drug-omics interaction landscapes may be systematically deconvolved thanks to deep learning-integrated multi-omics models like the MOVE framework(12). While apigenin coordinates glycolytic flux and autophagic clearance through AMPK/mTOR pathway crosstalk(13) and disrupts COX-2/PGE2-IL-6 inflammatory amplification loops(14) celastrol offers computational frameworks for the logical design of low-toxicity polyherbal formulations(3). When opposed to synthetic drugs, phytomedicines are more compatible with the gut microbiota. These results highlight the translational potential of phytopharmacology driven by multi-omics in overcoming treatment obstacles for colorectal cancer.

Anticancer drug discovery is being revolutionized by the integration of artificial intelligence with pharmaceutical research, which is changing the paradigm from conventional trial-and-error methods to computationally driven methodologies. Drug-target interaction prediction and cancer subtype categorization are made easier by the effective analysis of large-scale chemical and multi-omics data made possible by deep learning models such graph convolutional networks and multi-kernel learning(15). The combination of autoencoder-based representation learning and multi-kernel learning provides a robust framework for screening anticancer drugs from complicated herbal remedies, even when the active ingredients are unknown

(16). multi-kernel learning incorporates heterogeneous data sources, such as chemical structures, gene expression, and protein interaction networks, to improve predictive robustness, autoencoders extract latent features from high-dimensional omics data—such as metabolomic or transcriptomic profiles—to capture crucial bioactivity patterns (17), whereas multi-kernel learning incorporates disparate data sources, including chemical structures, gene expression, and protein interaction networks, so boosting prediction robustness. To compare plant-derived fractions and reference medications in a colon cancer model, we used transcriptome-based profiling in conjunction with Jaccard similarity, autoencoders, and multi-kernel learning. We used high-throughput RNA sequencing, differential expression analysis, co-expression networks, and pathway enrichment to screen 187 herbal extracts for dual-targeting phytochemicals that influence metastasis and inflammatory pathways. Proteomic validation and domain enrichment analysis further validated the anticancer pathways. In keeping with the multi-component, multi-target philosophy of network pharmacology and providing a modernized approach to conventional medicine, this work builds an AI-enhanced multi-omics framework to speed up the creation of natural product-based anticancer drugs.

2. Results

2.1Transcriptomics combined with deep learning to screen potential anti-cancer CHMs

We conducted high-throughput sequencing of 592 cDNA libraries, generating approximately 9.09 Tb of raw sequencing data comprising 60.6 billion raw reads with an average read length of 100 bp (Supplementary Table 2). All sequencing data were deposited in the NCBI Sequence Read Archive (PRJNA1118364). Comparative analysis revealed that 166 medicinal plant fractions exhibited significantly different expression profiles compared to the negative controls. The most pronounced differential gene expression was observed in *Pinus massoniana* Lamb., which demonstrated 1,688 DEGs, comprising 783 upregulated and 905 downregulated transcripts (Supplementary Fig. 4, e). This was followed by *Mahonia fortunei* (Lindl.) Fedde exhibited 493 upregulated and 731 downregulated DEGs (Supplementary Fig. 4, f). The results of the differential analysis of the other CHM fraction treatment groups and the negative control are shown in (Supplementary Fig. 4). The Jaccard indices for most medicinal herb crude extracts and anticancer medications were concentrated at low levels for the Jaccard similarity analysis (Fig. 1, a). Furthermore, there was a positive association between the Jaccard index and the quantity of differentially expressed genes (DEGs) (Fig. 1, b). The group with comparatively high matching to the transcriptome signatures of anticancer medications was represented by the top 30 herbs with the highest similarity across all samples (Fig. 1, c), Many herb samples had poor similarity scores according to the Autoencoder-based analysis (Fig. 1, d). A subset of herb samples, however, clustered with the positive control (anticancer medicine) samples, according to 2D visualization (Fig. 1, e). Interestingly, compared to other samples, the top 30 candidate herbs found using this method had much better similarity scores (Figure.1, f). The model combined the vanillact and rbfdot kernel functions for the Multiple Kernel Learning (MKL) analysis, both of which had comparatively large weights (Fig. 1, g). The top 30 candidates chosen by the MKL model showed noticeably higher similarity scores (Fig. 1, i), even though the similarity scores of all herb samples were generally low (Fig. 1, h). We found several candidates for medicinal herb crude extracts (e.g., DY-168: *Mahonia fortunei* (Lindl.) Fedde; DY-156: *Pinus massoniana* Lamb.) that showed relatively high matching to the transcriptomic signatures of anticancer drugs using the combined screening strategies (Jaccard similarity comparison, Autoencoder-based clustering, and MKL modeling). Notably, the intersection of the three screening methods screened a total of 27 potential anti-cancer CHMs (Supplementary Fig. 4, f). Through MTT assay-based screening using gradient concentration inhibition rates, we identified five candidate medicinal plants with stable pharmacological profiles in (Table 2).

2.2Functional enrichment analysis implicated DEGs in tumor progression and metastasis.

Chronic inflammation and carcinogenesis are closely related, according to recent research. Immune cells, whether local or recruited, are essential for regulating the TME along the course of cancer. To determine their biological pathways, networks,

and functional categories, DEGs were divided into up-regulated and down-regulated sets for functional enrichment analysis. The immune system (such as IL-17 and NOD-like receptors), signal transduction pathways (such as TNF, TGF-beta, NF-kappa B, JAK-STAT, MAPK, PI3K-Akt, ErbB, and Wnt), cell growth and death (including ferroptosis and necroptosis), and signaling molecules and interactions (particularly cytokine-cytokine receptor interactions) were the main areas in each treatment group. Moreover, the expression trend of DEGs in each signaling pathway was consistent with the positive control shown in (Fig. 2, a). For the three plants, *Geranium wilfordii* Maxim., *Pinus massoniana* Lamb., and *Typhonium giganteum* Engl., the up-regulated genes were predominantly associated with signal transduction and the immune system, as illustrated in (Fig. 2, b). In contrast, *Mahonia fortunei (Lindl.)* Fedde. and *Coptis chinensis* Franch. exhibited a stronger association with cell growth and death, as well as the immune system (Fig. 2, a). These processes are also closely related to environmental information processing and organismal systems, suggesting a potential connection to the similar effects of CHMs.

Most of the down-regulated genes were found in metabolic pathways such peroxisomes, terpenoid backbone biosynthesis, and the p53 signaling pathway, which is linked to cell development and death, as well as in lipid metabolism, namely in steroid and fatty acid production. (Supplemental Fig. 5, a-b). In the Gene Ontology (GO) enrichment analysis (Supplemental Fig. 5, c-d), the cellular component terms predominantly included extracellular space, vesicles, and exosomes. The molecular function terms were mainly related to transcription regulation, signal receptor/ligand binding, and enzyme regulation, particularly concerning redox enzymes. Additionally, the biological process terms were chiefly associated with macromolecular metabolism and cellular processes. Notably, within the molecular function of down-regulated genes, transmembrane transport and nucleotide binding were also significantly enriched.

2.3Screening of key genes during enrichment

Through transcriptomic profiling and pathway enrichment analysis of five medicinal plants (*Coptis chinensis* Franch., *Mahonia fortunei (Lindl.)* Fedde, *Pinus massoniana* Lamb., *Typhonium giganteum* Engl., *Geranium wilfordii* Maxim.) Compared to the positive control Sorafenib, we identified a subset of genes exhibiting concordant expression patterns (|logFC| >2) associated with key oncogenic pathways. Notably, LCN2 (lipocalin-2) demonstrated significant upregulation in *Coptis chinensis* Franch., *Pinus massoniana* Lamb., and *Mahonia fortunei (Lindl.)* Fedde., surpassing Sorafenib-induced levels (Supplementary Fig. 4, f). Mechanistically, LCN2 overexpression under iron-overloaded conditions promotes ferroptosis, a non-apoptotic cell death pathway driven by lipid peroxidation, mirroring Sorafenib's pro-oxidative antitumor effects(18). Among the upregulated genes, GDF15 (growth differentiation factor 15) and TRAF1 (TNF receptor-associated factor 1) were prominently elevated. GDF15 suppresses Raf/MEK/ERK signaling via TGF-β/Smad3-mediated inhibition of MEK and ERK phosphorylation, thereby attenuating proliferative signaling (19). Together with Sorafenib's pro-apoptotic actions, TRAF1 increases TNF-α-dependent mitochondrial apoptosis by modifying the NF-κB and JNK pathways(20). Furthermore, redox homeostasis is further reinforced by the overexpression of TXNRD1 (thioredoxin reductase 1), which indirectly reduces RAS-RAF-MAPK hyperactivation.

Down regulated genes implicated in cholesterol and mevalonate metabolism (HMGCS1, MSMO1, MVD, MVK, CYP51A1, and SCD) revealed expression trends that corresponded with the mechanism of Sorafenib (Supplementary Fig. 4, f). Cholesterol production is disrupted by CYP51A1 inhibition, which also affects Ras membrane location and downstream MAPK signaling(21). Ras prenylation and RAF activation are lessened when HMGCS1 is inhibited because farnesyl pyrophosphate production is decreased (22). Downregulation of MSMO1 causes endoplasmic reticulum stress and the unfolded protein response (UPR), which activates pro-apoptotic pathways such as CHOP and JNK. Depletion of cholesterol mimics the antiangiogenic effects of sorafenib via interfering with VEGFR/PDGFR membrane trafficking(23).Notably, downregulation of PDE4D (phosphodiesterase 4D) elevates intracellular cAMP levels, which activates PKA to suppress Raf/MEK/ERK phosphorylation and VEGFR2 signaling, thus synergizing with Sorafenib's kinase inhibition(24). These findings emphasize the shared tumor-suppressive pathways between plant-derived drugs and Sorafenib, primarily through MAPK pathway regulation, metabolic reprogramming, and ferroptosis activation. Further confirmation of these targets may provide innovative combinatorial tactics for colorectal cancer treatment.

2.4Modular co-expression network analysis identifies herbal fraction-associated gene clusters in CRC

To boost screening efficiency, we partitioned high-dimensional omics data into modules associated to herbal fractions using weighted gene co-expression network analysis (WGCNA) via the R program. A soft thresholding power of β = 8 was set to reconcile scale independence (mean connectivity < 0.1) and network structure (Supplementary Fig. 5, e), resulting in the formation of 23 unique modules (Supplemental Fig. 6, a) after merging at a dissimilarity threshold of 0.2. Hierarchical clustering and trait heatmap analysis (Supplementary Fig. 5, f) found substantial relationships between modules herbal fractions: *Coptis*, *Mahonia*, and *Pinus* fractions were significantly connected with the royal blue module, whereas *Geranium* and *Sauromatum* fractions were aligned with the cyan module (Supplemental Fig. 6, a). We observed a positive correlation between module membership (MM) and gene significance (GS) using the scatter plot, suggesting that genes significantly associated with the treatment group are also important for essential modules (Supplemental Fig. 6, b). The royal blue module, which was enriched in MAPK pathway regulators (including GDF15 and TRAF1) and found hub genes associated with cancer staging, had a high intramodular connectivity (kME > 0.8) (Supplemental Table 5). Additionally, sorafenib-induced metabolic suppression was reflected in the downregulation of genes linked to cholesterol metabolism (CYP51A1, HMGCS1) in the cyan module (Fig. 3, a-b). Hub genes are given priority for CRC therapeutic targeting by this modular method, which successfully separates complex phytocompound-gene connections.

2.5Identification of hub genes and functional annotation within co-expression modules.

Strongly coupled nodes within co-expression modules (degree ≥ 20 and weight > 0.1) were identified as hub genes, producing 18 candidates in two primary modules. Network visualization using Cytoscape (v3.8.1) revealed divergent expression patterns: nodes in the cyan module were color-coded (Fig. 3, a) (orange: upregulated; purple: downregulated), whereas the royal blue module exhibited uniform connectivity (Fig. 3, b). Pathway divergence was revealed by functional enrichment analysis: the royal blue module dominated in amino acid metabolism and carbon/nitrogen cycling, while the cyan module was enriched in NF-κB signaling, antigen processing and presentation, TNF signaling, and fatty acid biosynthesis (KEGG, $p < 0.05$). Notably, the hub genes in the cyan module (AKAP12, NRP1, TXNRD1, FAM107B, and NT5E) revealed high relationships with the herbal fractions (Pearson's $r > 0.9$). The key regulator in all five herbal remedies was found to be the scaffolding protein AKAP12. By binding to Raf kinase and facilitating its interaction with inhibitory phosphatases (such PP2A), AKAP12 suppresses Raf/MEK/ERK signaling and downregulates Cyclin D1 to cause cell cycle arrest (25). NRP1, a co-receptor of VEGFR-2, competitively sequesters VEGF-A, therefore attenuating VEGFR-2 activation and angiogenesis(26). TXNRD1, a redox regulator, synergizes with Sorafenib-like drugs by suppressing RAS-RAF-MAPK hyperactivation via ROS scavenging. The links between the additional genes and essential pathways in both modules are indicated in (Fig. 3, c-d). These results highlight the usefulness of WGCNA in locating hubs responsive to phytocompounds, especially those that influence metabolic reprogramming and MAPK signaling (27).

2.6Dose-Response validation of CHMs efficacy in CRC suppression

Systematic MTT dose-response tests were carried out to confirm the herbal fractions' dose-dependent anti-proliferative effectiveness against cancer cells. The findings showed that herbal fractions significantly inhibited the proliferation of colorectal cancer cells in a dose-dependent manner, with fractions from *Geranium wilfordii* Maxim. and *Pinus massoniana* Lamb. showing the strongest anti-proliferative activity (Fig. 3, e). Notably, the dose-response curves revealed exceptional stability over the biological replicates. At a dose of 25 μg/mL, *Pinus massoniana* Lamb. and *Geranium wilfordii* Maxim. both demonstrated 50% growth inhibition, demonstrating their higher therapeutic potential. Conversely, the fractions of *Coptis chinensis* Franch. showed a half-maximal inhibitory concentration (IC50) of 160 μg/mL, indicating substantial cytotoxicity. These results confirm the concentration-responsive bioactivity of the chosen herbal fractions and demonstrate *Pinus massoniana* Lamb's potential as a particularly appealing option for additional anti-neoplastic drug development. The

consistent dose-response correlations demonstrate the pharmacological stability of these natural compounds and point to their potential translational utility in precision oncology.

2.7Proteomics data quality control

This work employed transcriptomics to screen the CHMs and identify potential anti-cancer targets. After that, proteome confirmation was done using DIA mass spectrometry. Over 8,000 proteins were assessed in each sample, and proteomic analysis identified 120,186 unique peptides (Supplemental Fig. 7, a). Nearly 90% of the proteins in each group overlapped with biological replicates, indicating good concordance between technical replicates, according to Venn diagram analysis (Supplemental Fig. 7, e). Strong analytical reproducibility across the sample groups was shown by the quantitative distribution patterns and span curves (Supplemental Fig. 7, b). Normalized box plots showed good normalization efficacy and efficient data calibration, with adjusted medians converging around zero on the vertical axis. (Supplemental Fig. 7, c). Supervised partial least squares discriminant analysis (PLS-DA) was employed to mitigate potential model bias resulting from considerable inter-group variability. Permutation testing demonstrated that this multivariate method effectively distinguished sample clusters and maintained model robustness. (Supplemental Fig. 7, d) The integrated multi-omics approach displayed solid analytical performance in finding treatment candidates and explaining their biological mechanisms through complementing transcriptome-proteome correlation analysis.

2.8Proteomic profiling identifies cancer pathway alterations via comparative analysis

Quantitative proteomic analysis was accomplished by scanning databases of raw mass spectrometry data to derive peptide detection signal intensities, which permitted the calculation of protein-level quantification. The same proteins between samples were quantitatively compared following sample normalization. Effective data filtering and missing value imputation based on sample groupings aided the measurement of protein abundance ratio distribution within the control groups. As shown in (Fig. 4, a). statistical analysis of differentially expressed proteins (DEPs) across fractionated experimental groups and negative controls identified 8,539 significant DEPs (4,687 upregulated; 3,852 downregulated). Every experimental group and the positive control showed similar increasing and downward trends in DEP expression. (Fig. 4, b).

Analysis of KEGG pathways demonstrated alterations in cancer-related pathways among the DEPs. Upregulated proteins were predominantly found in pathways connected to ferroptosis, TNF signaling, IL-17 signaling, apoptosis, HIF-1 signaling, and p53 signaling. (Fig. 4, c). Distinct pathway signatures were identified in herb-specific downregulated proteins: fractions from *Coptis chinensis* Franch., *Mahonia fortunei (Lindl.)* Fedde and *Pinus massoniana* Lamb. exhibited enrichment in retrograde endocannabinoid signaling, chemical carcinogenesis-ROS, and cytochrome P450-mediated drug metabolism (Fig. 4, d). DEPs associated with *Typhonium giganteum* Engl. were clustered in pathways related to cell adhesion molecules, leukocyte transendothelial migration, steroid production, and Wnt signaling mechanisms, all of which are critical for the migration of cancer cells. Complement/coagulation cascades, lipid metabolism, and ECM-receptor interactions—pathways mechanistically connected to tumor angiogenesis and proliferation—were markedly elevated in *Geranium wilfordii* Maxim.

A substantial enrichment of downregulated proteins in domains associated with cell adhesion factors, such as V-set, Ig_3, C2-set_2, and I-set, was found by analyzing Pfams protein domains in differentially expressed proteins within each fraction group(28). These domains include immunoglobulin superfamily members and integrins. The decreased production of these proteins could disrupt intercellular adhesion and cell-matrix interactions, thus restricting tumor cell motility, invasion, and distant colonization, ultimately decreasing colorectal cancer metastasis. Furthermore, the presence of the EGF_CA domain in epidermal growth factor-related proteins suggests that lowering these proteins may disrupt critical signaling pathways necessary for cell survival and proliferation, particularly those reliant on the EGF receptor family like EGFR/HER signaling, thereby preventing the growth of tumor cells. (Fig. 4, e-f).

Significant agreement was found between the pathway enrichment patterns and the transcriptome profiling data (Supplementary Fig. 5, a-b), confirming the reliability of multi-omics in cancer-related pathway changes. The proteome

landscape of herbal fraction therapies is thoroughly characterized by these findings, which demonstrate the coordinated control of neoplastic pathways via both transcriptional and post-translational processes. The pathway signatures that have been found provide mechanistic insights into the possible anti-carcinogenic actions of herbal components.

2.9. Figures, Tables and Schemes

Table 1
Positive control drug information

Positive drug	Gradient dose	Starting dose	Product code	Specification	Manufacturer
Doxorubicin Hydrochloride	0.1/1/5/10(uM)	20mM	S17092-25mg	98%	Shanghai yuanye Bio-Technology Co., Ltd
Docetaxel	0.1/1/10/100/1000(uM)	20mM	D807092-250mg	98%	Guangzhou BaoHui Biomedical Technology Co., Ltd.
Gefitinib	0.1/1/5/10(uM)	20mM	G828597-1g	98%	Shanghai Macklin Biochemical Co., Ltd
HHT (Homoharringtonine)	0.1/1/10/100(nM)	20mM	H111922-20mg	≥ 98%	Shanghai Aladdin Biochemical Technology Co.,Ltd
gemcitabine	1/10/50/100(nM)	20mM	G824361	99%	Shanghai Macklin Biochemical Co., Ltd
Cisplatin	0.01/0.1/1/5/10/20(uM)	20mM	C14330-500mg	99%	Shanghai JiZhi Biochemical Technology Co., Ltd.
Lenvatinib	0.1/1/10/50(uM)	20mM	E856914-1g	99%	Shanghai Macklin Biochemical Co., Ltd
Benzenepropanoic acid	0.001/0.0002/0.00004/0.000008(uM)	20mM	P106869-250mg	99%	Shanghai Aladdin Biochemical Technology Co.,Ltd
Sorafenib	0.1/1/5/10(uM)	20mM	S125098-1g	≥ 99%	Shanghai Aladdin Biochemical Technology Co.,Ltd
Cabozantinib	5000/1000/100/10/1/0.1/0.01(nM)	500uM	S41123-10mg	≥ 99%	Shanghai yuanye Bio-Technology Co., Ltd

Table 2
List of candidate CHMs

Latin name	Family	Genus	Up-regulation genes	Down-regulation genes	Efficacy
Pinus massoniana Lamb.	Pinaceae	Pinus	387	471	Qi-regulating drug
Mahonia fortunei (Lindl.) Fedde	Berberidaceae	Mahonia	280	436	Heat-clearing and dampness-eliminating drug
Typhonium giganteum Engl.	Araceae	Sauromatum	256	244	Qi-regulating drug
Geranium wilfordii Maxim.	Geraniaceae	Geranium	230	250	Medicine for rheumatism
Coptis chinensis Franch.	Ranunculaceae	Coptis	223	325	Heat-clearing and dampness-eliminating drug

3. Discussion

CHM has grown into a comprehensive therapeutic paradigm supported by millennia of empirical evidence for disease prevention and treatment. Unlike the reductionist approaches widespread in Western medicine, CHM stresses the systemic regulation of host homeostasis to increase self-repair mechanisms and immunological competence, demonstrated by the "coexistence with tumors" technique in oncology(33). In CHM theory, CRC, also known as intestinal carcinoma (IC), is a pathophysiologic condition linked to heat-toxicity accumulation and Qi shortage. Qi-tonifying therapies are required because Qi disorders, which are defined by impaired primordial energy, induce cancer through the dysregulation of immunometabolism networks, according to emerging multi-omics investigations. Pharmacological investigations have validated the immunomodulatory efficacy of *Glycyrrhiza uralensis* Fisch(34)., *Astragalus membranaceus* (Fisch.) Bunge and Atractylodes macrocephala Koidz(35, 36)., which are rich in triterpenoid saponins, flavonoids and polysaccharides. These phytoconstituents exhibit dual anticancer action by blocking the NF-κB/STAT3 pathway and downregulation of PD-L1(37, 38). Simultaneously, heat toxicity clearance procedures using *Scutellaria barbata* D. Don. and *Hedyotis diffusa* Willd. showed CRC-suppressive effects through Nrf2-mediated oxidative stress mitigation and gut microbiota adjustment(39, 40).

The special benefits of CHM in overcoming the drawbacks of chemotherapeutics have been made clear by systems pharmacology techniques. By restoring the CXCL12/CXCR4 axis, Romanianize D corrects 5-FU-induced hematopoietic dysfunction(41) (Hong et al., 2023), Meanwhile, curcumin increases the effectiveness of oxaliplatin and bevacizumab through VEGF/PI3K-AKT crosstalk, concurrently lowering the cardiotoxicity linked to bevacizumab(42) (Villegas et al., 2021). Proteomic profiling further demonstrated that TCM formulations synergize with checkpoint inhibitors by reprogramming tumor-associated macrophages and increasing CD8 + T cell infiltration(43) (Qian et al., 2023). Drug resistance and off-target effects are two major issues in traditional oncology that are addressed by this change in the phototherapeutic paradigm from cytotoxic eradication to microenvironmental reprogramming. Future study merging metabolomic flux analysis with spatial transcriptomics will further unravel CHM's polypharmacological networks, ultimately enhancing the application of precision herbal medicine in CRC care.

Heat-clearing herbs, such as *Scutellaria barbata* D. Don. and *Lonicera japonica* Thunb., have been shown to suppress NF-κB-mediated inflammatory cascades, downregulate pro-inflammatory cytokines (TNF-α, IL-6), and induce mitochondrial-dependent apoptosis while inhibiting VEGF-driven angiogenesis(44) (Liu et al., 2024). Concurrently, qi-regulating botanicals (*Citrus reticulata* Blanco. and *Citrus aurantium* L) alter the COX-2/PGE2 axis to relieve gastrointestinal inflammation and reverse tumor-associated immunosuppression. Certain flavanones prevent inflammation-induced proliferation by inhibiting the STAT3 pathway(45, 46)(Rong et al., 2021; Lee et al., 2024).Anti-rheumatic drugs (*Typhonium giganteum* Engl., Geranium

wilfordii Maxim.), which are high in bioactive alkaloids and terpenoids, alleviate chronic inflammation by blocking the IL-1β/IL-17 axis and immunomodulating via Th17/Treg differentiation(47, 48) (Chitturi et al., 2023; Zhu et al., 2025).

Our high-throughput multi-omics platform identified five core candidates that align with CHM therapeutic principles for CRC: heat-clearing/dampness-drying agents (*Mahonia fortunei (Lindl.)* Fedde, *Coptis chinensis* Franch.), qi-regulating herbs (*Pinus massoniana* Lamb., *Typhonium giganteum* Engl.), and wind-damp dispelling species (*Geranium wilfordii* Maxim.) Notably, derivatives of *Mahonia fortunei (Lindl.)* Fedde. and *Coptis chinensis* Franch. (berberine analogs) demonstrated synergistic regulation of the PI3K/AKT and Wnt/β-catenin pathways in transcriptomic analysis. *Pinus massoniana* Lamb. *Typhonium giganteum* Engl. modulates immunometabolism via PPARγ/NF-κB crosstalk, while targeting cancer stemness markers (CD44+/CD133+) in proteomic profiling. The TCM approach of "clearing heat-toxin" and "regulating qi stagnation" in the treatment of intestinal neoplasia is supported by this phytochemical repertoire, which together address CRC pathogenesis through multifaceted mechanisms: inflammatory resolution, tumor microenvironment remodeling, and stemness suppression.

Transcriptomic profiling demonstrated that *Mahonia fortunei (Lindl.)* Fedde. strongly inhibits cholesterol production by SREBP2 downregulation, fatty acid synthesis via FASN and ACC1 repression, and oxidative phosphorylation, as evidenced by a decrease in electron transport chain complex proteins. Proteomic validation found the concurrent increase of lipid peroxidation drivers, notably ACSL4, demonstrating bidirectional modulation of metabolic homeostasis. Through ATP depletion via OXPHOS inhibition and membrane stability compromised by unsaturated fatty acid exhaustion, this dual-axis disruption mechanistically interrupts the neoplastic energy source and synergistically activates ferroptosis cascades through GPX4 suppression. Interestingly, colorectal cancer with a KRAS mutation shows increased metabolic dependence and ferroptosis susceptibility(49). Our findings point to a spatiotemporally coupled'metabolic collapse-death trigger' paradigm, in which escalating ATP depletion and lipid peroxidation form a self-amplifying pro-ferroptosis loop. Simultaneously, multi-omics analysis indicated a coordinated suppression of the DNA damage-immune axis, as evidenced by transcriptional downregulation of FANCD2 and proteomic reduction in ROS-scavenging CYP450 isoforms. This combination flaw lowers the ability to repair DNA while increasing genotoxic stress. Additionally, the immunosuppressive milieu is altered by the concurrent inhibition of IL-6/STAT3 signaling, which may increase immunogenic cell death(50).By decreasing HMGCR and SQLE and downregulating FASN and SCD1, *Coptis chinensis* Franch. dramatically reduces sterol biosynthesis and fatty acid desaturation. Since SCD1-mediated monounsaturated fatty acid (MUFA) production confers ferroptosis resistance in colorectal cancer (CRC) (51), transcriptional silencing of SCD1 in combination with elevated ACSL4 protein levels causes a lipidomic imbalance that encourages polyunsaturated fatty acid (PUFA) peroxidation, a typical ferroptosis trigger(52). Pharmacologically, geranylgeranyl pyrophosphate (GGPP) is depleted by HMGCR inhibition, which hinders KRAS membrane localization and the MAPK pathway's subsequent activation(53). Targeting FASN (lipogenesis), SCD1 (desaturation), and HMGCR simultaneously creates a threefold vulnerability: (1) restricting the availability of substrate for membrane biogenesis; (2) changing the lipid composition in favor of peroxidation-prone PUFA species; and (3) blocking oncogenic KRAS signaling. These phytochemicals are multitarget modulators of the metabolic plasticity of colorectal cancer, per integrative research. *Mahonia fortunei (Lindl.)* Fedde derivatives exploit the intrinsic connection between KRAS-driven anabolic metabolism and ferroptosis vulnerability. *Coptis chinensis* Franch. combines attacks on redox balance, oncogenic signaling, and lipidomic stability to create a therapeutic approach that aligns with the "metabolic synthetic lethality" idea. These findings imply that SREBP2, ACSL4, and SCD1 are pharmacologically actionable nodes for CRC combination therapies that focus on metabolic adaptation and cell death avoidance mechanisms.

Pinus massoniana Lamb. is identified by the thorough multi-omics research as a potent regulator of colorectal cancer (CRC) pathobiology through coordinated immunological and metabolic disruption. Transcriptomic profiling reveals a marked reduction of lipid metabolic networks, including terpenoid production and fatty acid metabolism. A reduction in the synthesis of unsaturated fatty acids provides proteomical evidence for this. Because CRC relies on lipid metabolic reprogramming to survive, this coordinated disruption destabilizes oncogenic lipid homeostasis by downregulating the transcription of master regulators PPARγ and SREBP1; pharmacological inhibition of ACC/FASN results in chemosensitization and lipotoxicity(54). Concurrent transcriptomic silencing of ROS scavenging pathways, particularly the NRF2/KEAP1 axis, along with proteomic

depletion of antioxidant enzymes (e.g., GPX4), precipitated lethal ROS accumulation. In addition to directly damaging genomes, elevated ROS also triggers ferroptosis cascades, which cooperate with transcriptional enrichments in the ferroptosis pathway. Significantly, p53-mutant SW480 cells displayed non-apoptotic death patterns, suggesting that oxidative stress and ferroptosis cooperate to overcome apoptosis resistance in p53-deficient colorectal cancer(55). Immune remodeling was demonstrated by the suppression of the IL-6/STAT3 axis, which decreases M2 macrophage polarization and PD-L1 expression and enhances cytotoxic T-cell infiltration—a behavior amplified by ROS-mediated immunogenic antigen release(56). Paradoxically, *Pinus massoniana* Lamb. upregulated SLC7A11, which boosts cystine-dependent antioxidant capacity, and HMOX1, which enhances cells' vulnerability to iron overload-induced ferroptosis. The redox rheostat of the orchestrate balances cytoprotective responses and pro-death signals. (21, 57). Concurrent reduction of CXCR4, which results in a glycolytic blockade, and WLS, which prevents Wnt/β-catenin signaling, disrupts metabolic plasticity. Furthermore, proteomic validation confirmed that SCD and RRM2 depletion causes nucleotide synthesis collapse and promotes lipid peroxidation(58, 59), which in turn results in immunogenic cell death and replication stress. These multi-target effects mechanistically converge along three axes: (1) immunological reactivation through suppression of PD-L1/STAT3; (2) redox crisis via interaction between ROS and ferroptosis; and (3) metabolic catastrophe via blockage of lipid/nucleotide synthesis. This three-way process resembles the concept of the "immunometabolism checkpoint," where metabolic therapies enhance immune-mediated tumor clearance. The regulatory nexus involving SREBP1, PPARγ-STAT3, and STAT3 elicited by *Pinus massoniana* Lamb. demonstrates phytochemicals' ability to simultaneously target oncogenic signaling, cell death pathways, and immunosuppression, signifying a paradigm shift from single-target treatments. *Typhonium giganteum* Engl. *Ty*phonium giganteum Engl. has polypharmacological efficacy against KRAS-mutant colorectal cancer through immunometabolism reprogramming, ferroptosis sensitization, and a coordinated activation of apoptosis and senescence. Proteomic validation of altered Ras membrane location due to prenylation blockade confirms the considerable suppression of mevalonate-cholesterol production and amino acid metabolism observed by multi-omics interrogation. Mechanistically, SAM depletion causes H3K27me3 demethylation, which epigenetically silences Wnt/β-catenin targets such as c-MYC and CCND1(60), On the other hand, fatty acid oxidation is disrupted by PPAR axis inhibition, which results in a glycolytic dependence that raises metabolic stress and initiates AMPK-Foxo-mediated apoptosis(61).The reduction of APCDD1/PTK7 and the transcriptional increase of AKAP12 and NR2F2 create a dual mechanism of Wnt inhibition. AKAP12 maintains stemness through PKC/STAT3 signaling(62), but Wnt ligand activation is reduced by APCDD1/PTK7 downregulation(63). Proteomic analyses verified that β-catenin targets were repressed and that SCD, which causes lipid peroxidation, was suppressed(58). Furthermore, the leucine-mTORC1 axis is disrupted by SLC7A5 inhibition, which increases immunogenicity. Ironically, TRAF1 upregulation inhibits pro-inflammatory cytokines (IL-6/TNF-α) mediated by NF-κB(64), whilst DKK4 downregulation decreases MDSC infiltration driven by Wnt/Ca^{2+}(65). The concurrent decrease of PD-L1 and rise of Granzyme B in proteomic datasets supports $CD8^+$ T-cell activation. In SW480 models, these multi-tiered effects—which include immunological potentiation, metabolic sabotage, and epigenetic reprogramming—combine to overcome KRAS-driven treatment resistance, proving that phytochemicals can address the multifaceted adaptability of CRC.

According to multi-omics research, *Geranium wilfordii* Maxim. produces anti-CRC effects by coordinated Wnt pathway inhibition, TME reconfiguration, and metabolic intervention. The transcriptional rise of CAV1 (Caveolin-1) inhibits the NF-κB signaling axis, suppresses angiogenesis by modifying endothelial dysfunction, and reduces the release of pro-inflammatory cytokines (IL-6/TNF-α) (66). Concurrent elevation of ICAM1 enhances immunoediting and promotes the formation of immunological synapses between cytotoxic lymphocytes and cancerous cells(67). Mechanistically, elevation of TRAF1 inhibits NF-κB-mediated resistance to apoptosis, while upregulation destabilizes ZFP36L1 pro-survival genes (Bcl-2, MCL1) via mRNA degradation(45). By preventing urokinase plasminogen activator (uPA)-driven extracellular matrix degradation, proteomic overexpression of SERPINB2 (PAI-2) lowers the risk for metastasis(68). These multilayered effects, which include matrix stabilization, immunological potentiation, and inflammatory control, collectively slow the progression of colorectal cancer through TME-centric pharmacodynamic activities.

4. Materials and Methods

4.1 Extracts Plant materials and sample preparation

A total of 187 Chinese herbal medicine materials were provided by the National Engineering Research Center for Southwest Endangered Medicinal Materials Resources Development and the Guangxi Key Laboratory of Medicinal Resources Protection and Genetic Improvement, Guangxi Botanical Garden of Medicinal Plants, Nanning, China. All materials, originated from cultivated or institutionally maintained collections rather than wild populations. No wild plants were collected by the authors, so a field collection permit was not required. The materials were obtained and used in accordance with relevant institutional and national regulations. They were detailed information is provided in Supplementary Table 1. The materials were ground into fine powders and assigned identifiers according to their extraction methods. Samples labelled “D” were prepared by hot-water steeping and lyophilization. “GX” samples underwent ethanol extraction, resin-column purification, and vacuum concentration, whereas “S” samples were produced by supercritical CO_2 extraction followed by solvent extraction and vacuum drying. Detailed procedures are shown in Supplementary Fig. 3. the 187 materials were classified into 20 groups according to their pharmacological properties. Ten commercial anticancer drugs served as positive controls, while DMSO was used as the negative control. All test samples were dissolved in DMSO before anticancer bioassays. Information on the controls is provided in Table 1, and the overall study workflow is presented in Supplementary Fig. 1.

4.2 Cell culture and drug preparation

The SW480 colon cancer cell line utilized in this study is a commercially available cell line consisting of standard laboratory strains devoid of human genetic material. The experimental procedures adhered to institutional ethical standards and conformed to the regulations of China's Human Genetic Resources Administration. The human colorectal adenocarcinoma cell line SW480 was obtained from the Kunming Cell Bank of Type Culture Collection, Kunming Institute of Zoology, Chinese Academy of Sciences, Kunming, China.The cells were cultured in Dulbecco's Modified Eagle Medium (DMEM) supplemented with 10% fetal bovine serum (FBS) and maintained at 37°C in a 5% CO_2 atmosphere. Subculturing was conducted upon reaching 80–90% confluency using 0.125% trypsin for cell detachment. A typical viability assay was used to assess cell viability 24 hours after treatment. 187 medicinal plant extracts were first screened at a concentration of 100 μg/mL, and subsequent modifications were made in accordance with viability standards. Aiming for a cell viability of roughly 80%, screening doses for transcriptome sequencing were established. The medicinal plant was designated as the experimental group, the anticancer medication as the positive control group, and 0.1% DMSO was administered to the negative control group.

4.3 Cellular MTT assay

After seeding SW480 cells at a density of 5×10^3 cells per well in 96-well plates, the cells were incubated for a full day before being treated with either BRPS or Sorafenib (5 μg/mL) as a positive control. Cell viability was assessed using the MTT test with absorbance at 490 nm after an additional 24 hours(69).

4.4 Transcriptomic sequencing analysis

Total RNA was extracted using the FastPure Plasmid Mini Kit, and RNA integrity was verified using the NanoDrop 2000 and Agilent 2100 Bioanalyzer (RIN > 8, OD260/280: 1.8–2.0). Following the construction of cDNA libraries using the MGIEasy kit, the BGISEQ-2000 platform was used for sequencing, producing 100 bp paired-end reads. (Supplemental Fig. 2). FastQC and Trimmomatic were used to control the quality of the sequencing data, (Supplemental Table 3) provides comprehensive quality metrics. The cleaned data were stored in the NCBI Sequence Read Archive (SRA) following quality control and adapter cutting.

RNA-seq data were analyzed using the "New Tuxedo" pipeline, with HISAT(15) employed for alignment, StringTie(70) for transcript assembly and quantification, and DESeq2 for differential expression analysis (Supplemental Fig. 2). Differentially expressed genes (DEGs) were defined as having a p-value ≤ 0.05 and |log2FC| ≥1 (71). A comparative analysis was conducted involving 187medicinal plant groups, alongside positive and negative controls, to identify genes associated with antitumor activity. Gene Ontology (GO) enrichment analysis of differentially expressed proteins (DEPs) and DEGs was

performed using the GOseq R package, based on the Wallenius noncentral hypergeometric distribution(72) (http://geneontology.org/). Pathway analysis of DEPs and DEGs was conducted using the KEGG database(32) (http://www.kegg.jp/), with the statistical enrichment of DEGs in KEGG pathways assessed using KOBAS software(73). Gene Ontology and KEGG pathway analyses (cluster Profiler) highlighted inflammation and metastasis pathways, with expression visualized via TBtools heatmaps. The full pipeline details are provided in (Supplemental Table 3).

4.5 Machine Learning-Based Screening of Medicinal Plants

By comparing sets of significantly differentially expressed genes, Jaccard similarity analysis assesses the mechanistic similarity between Chinese herbal medicines and the positive control. The coefficient J (A, B) = |A∩B|/|A∪B| ranges from 0 to 1, with values closer to 1 indicating greater similarity. A similarity threshold of Jaccard coefficient ≥ 0.3 was employed in this study(74). We used a combined gene expression matrix as input and 178 transcriptome profiles, each of which contained gene-level data like logFC, P-value, and adj.P.Val. An autoencoder (AE) model was developed to assess the mechanistic similarities between sorafenib and each plant extract (17). With a symmetrical encoder-decoder construction, the autoencoder (AE) was developed to carry out nonlinear dimensionality reduction. This is achieved by transforming high-dimensional logFC feature vectors into a lower-dimensional latent space and then recreating the original input. The mean squared error between the input and reconstructed output was decreased by the training. Next, the optimal linear combination of a linear kernel based on the original features and a radial basis function (RBF) kernel created from the latent features was found using multiple kernel learning (MKL)(75). Similarity between each plant extract and sorafenib was quantified as the corresponding element in the fused kernel matrix. Results from both analytical approaches are presented in Fig. 1.

4.6 Weighted gene co-expression network analysis (WGCNA)

We used WGCNA version 1.73 in R version 4.0 to build a weighted co-expression network, detecting 21 modules using a soft threshold of $\beta = 7$ (scale-free $R^2 = 0.85$). Analysis of functional enrichment in these modules uncovered significant cancer-related pathways, and the hub genes were displayed in Cytoscape version 3.8.1(76, 77). With a degree threshold of ≥ 20, particularly in the cyan and royal blue modules, hub genes identified could potentially be targeted for cancer therapy. Analysis steps, software used, and primary scripts in our pipeline are detailed in Supplemental Table 3.

4.7 Proteomic analysis

Proteomic analysis was performed on lysates from fraction-treated cells utilizing 2% sodium deoxycholate (SDC) and 100 mM Tris-HCl (pH 8.5), followed by sonication and centrifugation at 12,000 × g for 5 min. Protein concentrations were determined using the bicinchoninic acid (BCA) assay. Twenty microliters of protein samples were enzymatically digested with the QLBIO MagicOmics-MMB8X proteomic digestion kit by incubating with MMB beads at 37°C for 30 min. Subsequently, 45 µL of binding buffer was introduced, and the mixture was agitated at room temperature for 15 min. The beads were resuspended in 40 µL of enzyme working solution and incubated for at least 4 hours at 37°C after three washes with wash buffer. 5 µL of termination buffer was added before lyophilization to stop the reaction.

Peptide samples were analyzed using a timsTOF_Pro2 mass spectrometer in the data-independent acquisition (DIA) mode. High-resolution mass spectrometry (MS) was used to achieve a resolution of 60,000 at 1222 across a m/z range of 100–1700. With 50 MS accumulations, an ESI voltage of 1.5 kV, and TIMS separation parameters set at 0.60–1.60 $cm^2/(V·s)$, the analysis yielded comprehensive spectrum coverage in cycles of 1.23 seconds. The UniProt Human Proteome Reference Database and Spectron software were used to process the mass spectrometry data. Methionine oxidation and N-terminal acetylation were changeable changes, while cysteine carbamidomethylating and trypsin/P digestion were permanent changes. Three technical duplicates of each sample were used in the analysis of the data using GraphPad Prism 7. With statistical significance criteria set at **** $p < 0.0001$, *** $p \le 0.001$, ** $p \le 0.01$, and * $p \le 0.05$, mean comparisons were carried out using least significant differences (LSDs). The article's results were shown mostly using software such as R (version 4.4.3), TB-tools (version 2.315), and the web portal Weishangxin.

5. Conclusions

Through metabolic reprogramming, ferroptosis activation, and immunomodulation, this work shows that specific Chinese herbal medicines, namely *Pinus massoniana* Lamb., *Mahonia* fortunei, and Coptis chinensis, have multi-target anti-CRC benefits. Integrative multi-omics analysis demonstrated coordinated inhibition of carcinogenic pathways (e.g., cholesterol production, IL-6/STAT3) and activation of lipid peroxidation-induced cell death. The identified hub genes and pathways emphasize the potential of CHMs as precision oncology medicines targeting CRC heterogeneity and therapy resistance. These results offer a strong basis for creating combination treatments based on phytochemicals to combat colorectal cancer.

Abbreviations

The following abbreviations are used in this manuscript:

Abbreviation	Full term
CHM	Chinese herbal medicine
TGF-β	Transforming Growth Factor-beta signaling pathway
CRC	Colorectal cancer
ESCC	Esophageal Squamous Cell Carcinoma
DLBCL	Diffuse Large B-Cell Lymphoma
MAPK	Mitogen-Activated Protein Kinase signaling pathway
NF-κB	Nuclear Factor Kappa-light-chain-enhancer of Activated B cells signaling pathway
TNF	Tumor Necrosis Factor
IL-17	Interleukin-17
cAMP	Cyclic Adenosine Monophosphate
cGMP-PKG	Cyclic Guanosine Monophosphate-Protein Kinase G
p53	Tumor Protein p53
PI3K/AKT	Phosphoinositide 3-Kinase/Protein Kinase B
AMPK	AMP-Activated Protein Kinase
RIG-I-like	Retinoic Acid-Inducible Gene I-like
NOD-like	Nucleotide-Binding Oligomerization Domain-like
PD-L1	Programmed Death-Ligand 1
Toll-like	Toll-like Receptor
JAK-STAT	anus Kinase-Signal Transducer and Activator of Transcription
VEGF	Vascular Endothelial Growth Factor
Wnt	Wingless/Integrated
EGFR	Epidermal Growth Factor Receptor
AP-1/BTG	Activator Protein 1/B-cell Translocation Gene signaling pathway
DMSO	Dimethyl Sulfoxide
DMEM	Dulbecco's Modified Eagle Medium
FBS	Fetal bovine serum
MTT	3-(4,5-Dimethylthiazol-2-yl)-2,5-diphenyltetrazolium bromide assay
BRPS	Bicinchoninic Acid Reducing Protein Assay
AnnexinV-FITC/PI	Annexin V-Fluorescein Isothiocyanate/Propidium Iodide staining
DEG	Differentially Expressed Genes
DEP	Differentially Expressed Protein
GO	Gene Ontology
KEGG	Kyoto Encyclopedia of Genes and Genomes
WGCNA	Weighted gene coexpression network analysis

SDC	Sodium deoxycholate
BCA	Sicinchoninic acid
TCEP	Tris (2-carboxyethyl) phosphine
CAA	Chloroacetamide
DIA	Data-Independent Acquisition
LSDs	least significant differences
TME	tumor microenvironment
PKAs	protein kinases
CAFs	cancer-associated fibroblasts
EPACs	exchange proteins activated
NAFLD	nonalcoholic fatty liver disease
EMT	epithelial-mesenchymal transition
PCA	Principal component analysis

Declarations

Conflicts of Interest:

The authors declare no conflict of interest.

Funding:

This work was supported by 1. Guangxi Natural Science Foundation Program (2023GXNSFBA026354) 2. Guangxi Scientific research and technology development program project (Guikezhong1598005-14) 3. Guangxi Key Laboratory of Medicinal Resources Protection and Genetic Improvement (KL2022ZZ01).

Author Contribution

Tingting Hao: Methodology, Supervision, Writing-original draft and visualization; Ya Ning: Investigation and Resources; Zhu Qiao: Data curation and Methodology; Dawei Li: Writing-review & editing. Die Jiang, Xingzhi Yang: Formal analysis, Investigation; Xing Jiang, Wenqing Su, Wendong He: Investigation; Xiaolei Zhou, Dandan Mo, Xuzhen Li: Resources; Xianghua Xia: Resources and Fund-ing acquisition; Qiang-qiang Zhu, Qinghua Kong: Resources; Yang Dong: Conceptualization, Methodology, Project administration; Xiaonan Yang: Data curation, Resources and Funding acquisition; Weibin Wang: Software,validation,Data curation and Writing-review & editing. All authors reviewed and approved the final manuscript.

Acknowledgement

The authors gratefully acknowledge the Guangxi Botanical Garden for providing authenticated medicinal plant materials and technical support in sample preparation.

Data Availability

Data Availability Statement: The transcriptomic sequencing data generated in this study have been deposited in the National Center for Biotechnology Information Sequence Read Archive under BioProject accession PRJNA1118364. The mass spectrometry proteomics data have been deposited with the ProteomeXchange Consortium via the iProX partner repository under accession IPX0012285001 (https://www.iprox.cn/page/subproject.html?id=IPX0012285001).(78).

References

1. Zhou, X., Khan, S., Huang, D. & Li, L. V-set and immunoglobulin domain containing (VSIG) proteins as emerging immune checkpoint targets for cancer immunotherapy. *Front. Immunol.* **13**, 938470. 10.3389/fimmu.2022.938470 (2022).
2. Mathiyalagan, R. et al. Triterpenoid saponin-based supramolecular host-guest injectable hydrogels inhibit the growth of melanoma via ROS-mediated apoptosis. *Mater. Sci. Eng. R.* **160**, 100824. 10.1016/j.mser.2024.100824 (2024).
3. Chitturi, P. et al. Tripterygium wilfordii derivative celastrol, a YAP inhibitor, has antifibrotic effects in systemic sclerosis. Ann. Rheum. Dis. 82, 1191–1204;10.1136/ard--223859(2023). (2023).
4. Yamamoto, H. et al. TRAF1 is critical for DMBA/solar UVR-induced skin carcinogenesis. J. Invest. Dermatol. 137, 1322–1332;10.1016/j.jid.12.026(2017). (2016).
5. Kanehisa, M. Toward understanding the origin and evolution of cellular organisms. Protein Sci. 28, 1947–1951;10.1002/pro.3715 (2019).
6. Liu, Y. et al. Three anti-inflammatory polysaccharides from Lonicera japonica Thunb.: insights into the structure-function relationships. Food Sci. Hum. Wellness 13, 2197–2207;10.26599/FSHW.9250183(2024). (2022).
7. Liu, Q. et al. Thioredoxin reductase 3 suppression promotes colitis and carcinogenesis via activating pyroptosis and necrosis. Cell. Mol. Life Sci. 79, 106;10.1007/s00018-022-04155-y (2022).
8. Zhao, M. et al. Targeting MAPK14 by lobeline upregulates Slurp1-mediated inhibition of alternative activation of TAM and retards colorectal cancer growth. Adv. Sci. 12, 2407900;10.1002/advs.202407900 (2025).
9. Zhang, Q. et al. Systems pharmacology–based dissection of anti-cancer mechanism of traditional Chinese herb Saussurea involucrata. Front. Pharmacol. 12, 678203;10.3389/fphar.678203(2021). (2021).
10. Briscik, M., Tazza, G., Vidács, L., Dillies, M. A. & Déjean, S. Supervised multiple kernel learning approaches for multi-omics data integration. BioData Min. 17, 53;10.1186/s13040-024-00406-9 (2024).
11. Zhu, Q. et al. Study on the mechanism of Jieduquyuziyin prescription improving the condition of MRL/lpr mice by regulating T cell metabolic reprogramming through the AMPK/mTOR pathway. *J. Ethnopharmacol.* **345**, 119584. 10.1016/j.jep.2025.119584 (2025).
12. Li, S. et al. Study on the mechanism of action of effective monomeric, berberine of Xianglian pill in inhibiting human colon cancer cells based on fatty acid synthase target. *J. Tradit Complement. Med.* **13**, 538–549 ; 10.1016/j.jtcme.2023.05.008(2023).
13. Pertea, M. et al. StringTie enables improved reconstruction of a transcriptome from RNA-Seq reads. *Nat. Biotechnol.* **33**, 290. 10.1038/nbt.3122 (2015).
14. Zhang, L. et al. Sorafenib triggers ferroptosis via inhibition of HBXIP/SCD axis in hepatocellular carcinoma. *Acta Pharmacol. Sin* **44**, 622–634 ; 10.1038/s41401-022-00981-9(2023).
15. Zhou, H. et al. SLC25A17 inhibits autophagy to promote triple-negative breast cancer tumorigenesis by ROS-mediated JAK2/STAT3 signaling pathway. *Cancer Cell. Int.* **24**, 85 ; 10.1186/s12935-024-03270-z(2024).
16. Cai, X., Yao, Z., Li, L. & Huang, J. Role of DKK4 in tumorigenesis and tumor progression. *Int. J. Biol. Sci.* **14**, 616–621. 10.7150/ijbs.24329 (2018).
17. Zuo, Z. et al. Ribonucleotide reductase M2 (RRM2): regulation, function and targeting strategy in human cancer. *Genes Dis.* **11**, 218–233 ; 10.1016/j.gendis.2022.11.022(2022).
18. Pope, L. E. & Dixon, S. J. Regulation of ferroptosis by lipid metabolism. *Trends Cell. Biol.* **33**, 1077–1087. 10.1016/j.tcb.2023.05.003 (2023).

19. Wen, C. & Xiaoqing, Z. Protective effect of notoginsenoside and tanshinone IIA on inflammation-related colorectal cancer mice and the inhibition effect on COX-2 expression. *Digit. Chin. Med.* **4**, 54–63 ; 10.1016/j.dcmed.2021.03.007(2021).
20. Dierge, E. et al. Peroxidation of n-3 and n-6 polyunsaturated fatty acids in the acidic tumor environment leads to ferroptosis-mediated anti-cancer effects. *Cell. Metab.* **33**, 1701–1715e 5; 10.1016/j.cmet.2021.05.016(2021).
21. Cao, M. et al. PDE4D targeting enhances anti-tumor effects of sorafenib in clear cell renal cell carcinoma and attenuates MAPK/ERK signaling in a CRAF-dependent manner. *Transl Oncol.* **19**, 101377. 10.1016/j.tranon.2022.101377 (2022).
22. Liu, Y. & Gu, W. p53 in ferroptosis regulation: the new weapon for the old guardian. *Cell. Death Differ.* **29**, 895–910 ; 10.1038/s41418-022-00943-y(2022).
23. Koch, S. et al. NRP1 presented in trans to the endothelium arrests VEGFR2 endocytosis, preventing angiogenic signaling and tumor initiation. *Dev. Cell.* **28**, 633–646. 10.1016/j.devcel.2014.02.010 (2014).
24. Dimitrakopoulos, C. et al. Network-based integration of multi-omics data for prioritizing cancer genes. *Bioinformatics* **34**, 2441–2448. 10.1093/bioinformatics/bty148 (2018).
25. Atanasov, A. G., Zotchev, S. B., Dirsch, V. M. & Supuran, C. T. Natural products in drug discovery: advances and opportunities. *Nat. Rev. Drug Discov* **20**, 200–216 ; 10.1038/s41573-020-00114-z(2021).
26. Dai, S. L., Pan, J. Q. & Su, Z. R. Multi-omics features of immunogenic cell death in gastric cancer identified by combining single-cell sequencing analysis and machine learning. *Sci. Rep.* **14**, 21751 ; 10.1038/s41598-024-73071-x(2024).
27. Wang, L., Wang, H. & Fu, G. Multi-Nyström method based on multiple kernel learning for large scale imbalanced classification. Comput. Intell. Neurosci. 9911871; (2021). 10.1155/2021/9911871(2021).
28. Sherekar, S., Todankar, C. S. & Viswanathan, G. A. Modulating the dynamics of NFκB and PI3K enhances the ensemble-level TNFR1 signaling mediated apoptotic response. *npj Syst. Biol. Appl.* **9**, 1–13 ; 10.1038/s41540-023-00318-0(2023).
29. Lerner, E., Hamilton, A. & Sebti, S. Mini-review. Inhibition of Ras prenylation: a signaling target for novel anti-cancer drug design. Anti-Cancer Drug Des. 12, 229–238. PMID: 9199657 (1997).
30. Faubert, B., Solmonson, A. & DeBerardinis, R. J. Metabolic reprogramming and cancer progression. *Science* **368**, eaaw5473. 10.1126/science.aaw5473 (2020).
31. Lu, C. & Thompson, C. B. Metabolic regulation of epigenetics. *Cell. Metab.* **16**, 9–17. 10.1016/j.cmet.2012.06.001 (2012).
32. Xu, Z. et al. Mecheliolide elicits ROS-mediated ERS driven immunogenic cell death in hepatocellular carcinoma. *Redox Biol.* **54**, 102351. 10.1016/j.redox.2022.102351 (2022).
33. Kalli, M. et al. Mechanical compression regulates brain cancer cell migration through MEK1/Erk1 pathway activation and GDF15 expression. *Front. Oncol.* **9**, 992. 10.3389/fonc.2019.00992 (2019).
34. Hong, M. et al. Martynoside rescues 5-fluorouracil-impaired ribosome biogenesis by stabilizing RPL27A. *Sci. Bull.* **68**, 1662–1677. 10.1016/j.scib.2023.07.018 (2023).
35. Živalj, M., Van Ginderachter, J. A. & Stijlemans, B. Lipocalin-2: a nurturer of tumor progression and a novel candidate for targeted cancer therapy. *Cancers* **15**, 5159. 10.3390/cancers15215159 (2023).
36. Jiao, G. et al. Limitations of MTT and CCK-8 assay for evaluation of graphene cytotoxicity. *RSC Adv.* **5**, 53240–53244. 10.1039/C5RA08958A (2015).
37. Kanehisa, M. & Goto, S. K. E. G. G. Kyoto Encyclopedia of Genes and Genomes. *Nucleic Acids Res.* **28**, 27–30. 10.1093/nar/28.1.27 (2000).
38. Kanehisa, M., Furumichi, M., Sato, Y., Matsuura, Y. & Ishiguro-Watanabe, M. KEGG: biological systems database as a model of the real world. *Nucleic Acids Res. 53*. D672–D677. 10.1093/nar/gkae909((2024).
39. Kanehisa, M., Goto, S., Sato, Y., Furumichi, M. & Tanabe, M. KEGG for integration and interpretation of large-scale molecular data sets. *Nucleic Acids Res.* **40**, D109. 10.1093/nar/gkr988((2011).
40. McDermaid, A., Monier, B., Zhao, J., Liu, B. & Ma, Q. Interpretation of differential gene expression results of RNA-Seq data: review and integration. Brief. Bioinform. 20, ; (2044). 10.1093/bib/bby067(2018).

41. Grivennikov, S. I. Inflammation and colorectal cancer: colitis-associated neoplasia. *Semin Immunopathol.* **35**, 229–244. 10.1007/s00281-012-0352-6 (2013).
42. Zhang, W. et al. ICAM-1-mediated adhesion is a prerequisite for exosome-induced T cell suppression. *Dev. Cell.* **57**, 329–343e7 ; 10.1016/j.devcel.2022.01.002(2022).
43. Wong, S. H. & Yu, J. Gut microbiota in colorectal cancer: mechanisms of action and clinical applications. *Nat. Rev. Gastroenterol. Hepatol.* **16**, 690–704 ; 10.1038/s41575-019-0209-8(2019).
44. Snaebjornsson, M. T., Janaki-Raman, S. & Schulze, A. Greasing the wheels of the cancer machine: the role of lipid metabolism in cancer. *Cell. Metab.* **31**, 62–76 ; 10.1016/j.cmet.2019.11.010(2020).
45. Zhou, J. et al. GPR37 promotes colorectal cancer against ferroptosis by reprogramming lipid metabolism via p38-SCD1 axis. *Apoptosis* **29**, 1988. 10.1007/s10495-024-02018-4(2024) (2001).
46. Qian, Y. et al. Ginger polysaccharide UGP1 suppressed human colon cancer growth via p53, Bax/Bcl-2, caspase-3 pathways and immunomodulation. *Food Sci. Hum. Wellness* **12**, 467–476 ; 10.1016/j.fshw.2022.07.048(2023).
47. Li, C. et al. Geometry-based molecular generation with deep constrained variational autoencoder. *IEEE Trans. Neural Netw. Learn. Syst.* **35**, 4852–4861. 10.1109/TNNLS.2022.3147790 (2024).
48. Li, X. et al. Flavonoids for gastrointestinal tract local and associated systemic effects: a review of clinical trials and future perspectives. *J. Adv. Res.* **66**, 101234 ; 10.1016/j.jare.2025.01.014(2025).
49. Jiang, L. et al. Ferroptosis as a p53-mediated activity during tumour suppression. *Nature* **520**, 57–62. 10.1038/nature14344 (2015).
50. Han, W. & Liu, J. Epigenetic silencing of the Wnt antagonist APCDD1 by promoter DNA hyper-methylation contributes to osteosarcoma cell invasion and metastasis. *Biochem. Biophys. Res. Commun.* **491**, 91–97 ; 10.1016/j.bbrc.2017.07.049(2017).
51. Ni, M. et al. Efficacy and safety of Shenbai granules for recurrent colorectal adenoma: a multicenter randomized controlled trial. Phytomedicine 127, 155496; (2024). 10.1016/j.phymed.2024.155496
52. Luo, Q. et al. Effects and mechanisms of anlotinib and dihydroartemisinin combination therapy in ameliorating malignant biological behavior of gastric cancer cells. Curr. Pharm. Biotechnol. 22, 523–533;10.2174/1389201021666200623132803 (2020).
53. Zhao, Q. et al. Effect of pristimerin on apoptosis through activation of ROS/endoplasmic reticulum (ER) stress-mediated Noxa in colorectal cancer. Phytomedicine 80, 153399;10.1016/j.phymed.153399(2021). (2020).
54. Overman, M. J. et al. Durable clinical benefit with nivolumab plus ipilimumab in DNA mismatch repair–deficient/microsatellite instability–high metastatic colorectal cancer. J. Clin. Oncol. 36, 773–779;10.1200/JCO.76.9901(2018). (2017).
55. Zhou, S., Xu, H., Tang, Q., Xia, H. & Bi, F. Dipyridamole enhances the cytotoxicities of trametinib against colon cancer cells through combined targeting of HMGCS1 and MEK pathway. Mol. Cancer Ther. 19, 135–146;10.1158/1535–7163.MCT-19-0413 (2020).
56. Anders, S. & Huber, W. Differential expression analysis for sequence count data. Genome Biol. 11, R106;10.1186/gb--11-10-r106(2010). (2010).
57. Westrick, R. J. et al. Deficiency of plasminogen activator inhibitor-2 results in accelerated tumor growth. J. Thromb. Haemost. 18, 2968–2975;10.1111/jth.15054 (2020).
58. Shannon, P. et al. Cytoscape: a software environment for integrated models of biomolecular interaction networks. Genome Res. 13, 2498;10.1101/gr.1239303 (2003).
59. Chen, F. et al. CYP51A1 drives resistance to pH-dependent cell death in pancreatic cancer. *Nat. Commun.* **16**, 2278. 10.1038/s41467-025-57583-2 (2025).
60. Villegas, C., Perez, R., Sterner, O., González-Chavarría, I. & Paz, C. Curcuma as an adjuvant in colorectal cancer treatment. Life Sci. 286, 120043;10.1016/j.lfs.120043(2021). (2021).

61. Kim, J., Park, S., Min, D. & Kim, W. Comprehensive survey of recent drug discovery using deep learning. Int. J. Mol. Sci. 22, 9983;10.3390/ijms22189983 (2021).
62. Siegel, R. L., Wagle, N. S., Cercek, A., Smith, R. A. & Jemal, A. Colorectal cancer statistics, 2023. CA Cancer J. Clin. 73, 233–254;10.3322/caac.21772 (2023).
63. Rong, X. et al. Citrus peel flavonoid nobiletin alleviates lipopolysaccharide-induced inflammation by activating IL-6/STAT3/FOXO3a-mediated autophagy. Food Funct. 12, 1305–1317;10.1039/D0FO02141E (2021).
64. Zhang, J. et al. Chinese herbal medicine for the treatment of intestinal cancer: preclinical studies and potential clinical applications. Mol. Cancer 23, 217;10.1186/s12943-024-02135-3 (2024).
65. Su, G., Morris, J. H., Demchak, B. & Bader, G. D. Biological network exploration with Cytoscape 3. Curr. Protoc. Bioinformatics 47, 8.13.1;10.1002/0471250953.bi0813s47 (2014).
66. Guarini, C., Grassi, T., Pezzicoli, G., Porta, C. & Beyond, R. A. S. and BRAF: HER2, a new actionable oncotarget in advanced colorectal cancer. Int. J. Mol. Sci. 22, 6813;10.3390/ijms22136813 (2021).
67. Salvatore, S. et al. Beware the Jaccard: the choice of similarity measure is important and non-trivial in genomic colocalisation analysis. Brief. Bioinform. 21, 1523–1530;10.1093/bib/bbz083 (2020).
68. Mao, X., Cai, T., Olyarchuk, J. G. & Wei, L. Automated genome annotation and pathway identification using the KEGG Orthology (KO) as a controlled vocabulary. Bioinformatics 21, 3787–3793;10.1093/bioinformatics/bti430 (2005).
69. Fan, M. et al. Atractylenolide I ameliorates cancer cachexia through inhibiting biogenesis of IL-6 and tumour-derived extracellular vesicles. J. Cachexia Sarcopenia Muscle 13, 2724–2739;10.1002/jcsm.13079 (2022).
70. Fu, R. et al. Apigenin remodels the gut microbiota to ameliorate ulcerative colitis. Front. Nutr. 9, 1062961;10.3389/fnut.1062961(2022). (2022).
71. Li, S. et al. Anti-tumor effects and mechanisms of Astragalus membranaceus (AM) and its specific immunopotentiation: status and prospect. J. Ethnopharmacol. 258, 112797;10.1016/j.jep.112797(2020). (2020).
72. Duan, H. et al. Anti-colorectal cancer actions of Glycyrrhiza uralensis Fisch. and its underlying mechanism via HPLC integration and network pharmacological approaches. Phytomedicine 138, 156370;10.1016/j.phymed.156370(2025). (2025).
73. Lee, K. I. et al. Alleviating depressive-like behavior in DSS-induced colitis mice: exploring naringin and poncirin from Poncirus trifoliata extracts. Biomed. Pharmacother. 175, 116770;10.1016/j.biopha.116770(2024). (2024).
74. Yildirim, M. et al. AKAP12/gravin gene expression in colorectal cancer: clinical importance and review of the literature. J. BUON 18, 635–640. PMID: 24065476 (2013).
75. Li, K. et al. AKAP12 promotes cancer stem cell-like phenotypes and activates STAT3 in colorectal cancer. Clin. Transl. Oncol. 25, 3263–3276;10.1007/s12094-023-03230-5 (2023).
76. Lin, M. C. et al. Ago2/CAV1 interaction potentiates metastasis via controlling Ago2 localization and miRNA action. EMBO Rep. 25, 2441–2478;10.1038/s44319-024-00132-7 (2024).
77. Blondy, S. et al. 5-Fluorouracil resistance mechanisms in colorectal cancer: from classical pathways to promising processes. Cancer Sci. 111, 3142–3154;10.1111/cas.14532 (2020).

Figures

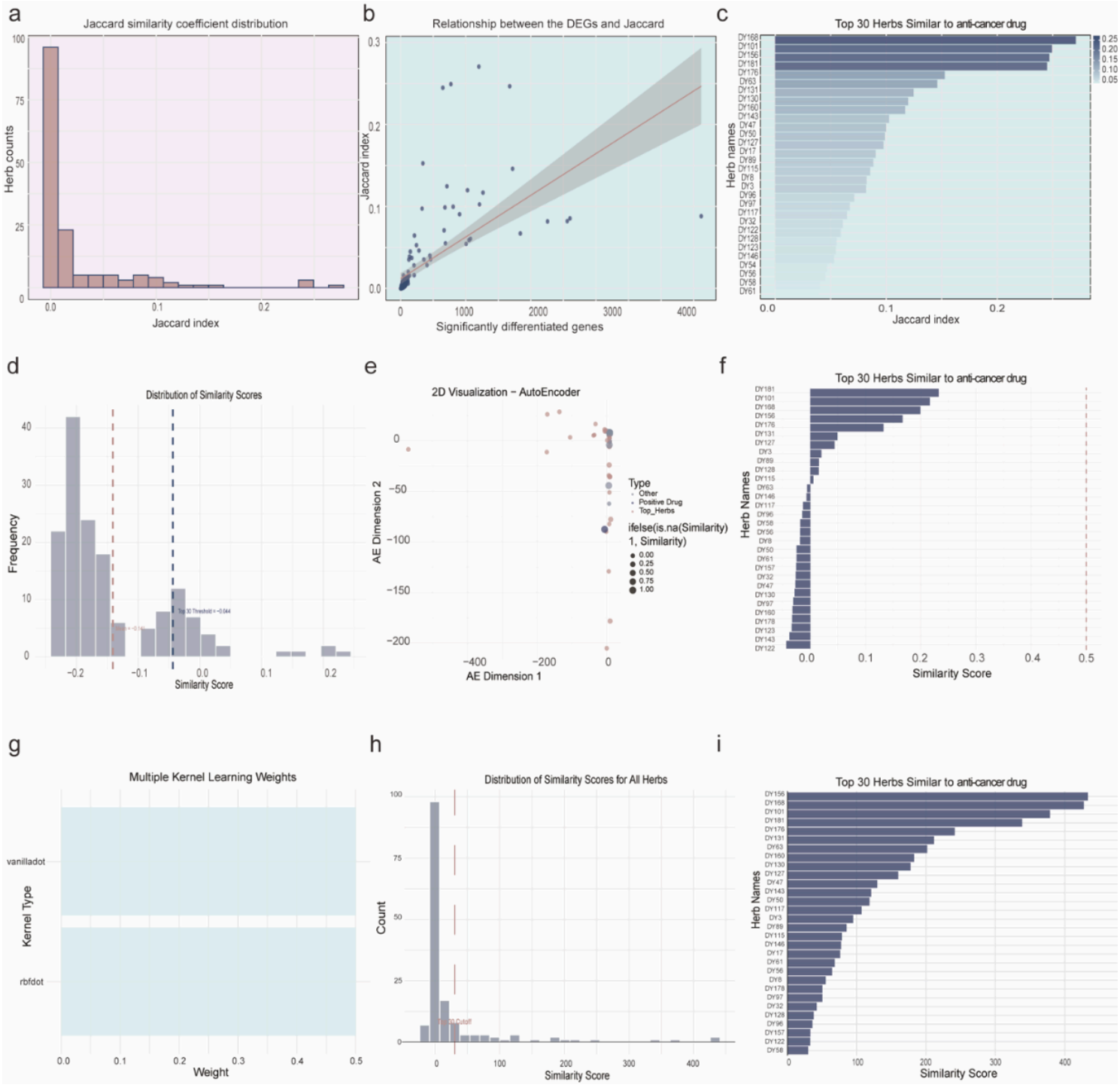

Figure 1

Deep learning combined with Jaccard to screen potential anti-cancer Chinese herbs. a: Distribution of Jaccard similarity coefficients between transcriptomic profiles of Chinese herbal extracts and the positive control anti-cancer drug (sorafenib). The x-axis indicates the Jaccard similarity coefficient; the y-axis shows the number of herbs at each similarity level. b: Scatter plot depicting the correlation between the number of significantly differentially expressed genes (x-axis) and the Jaccard similarity coefficient (y-axis) for each Chinese herbal extract relative to sorafenib. c: Top 30 herbs ranked by Jaccard similarity coefficient. The y-axis lists herb names, and the x-axis represents the similarity coefficient. Color gradient from light to dark reflects low to high similarity coefficients. d: Distribution of similarity scores (cosine similarity) between Chinese herbs and the positive control. The x-axis shows similarity scores; the y-axis indicates frequency (number of herbs). Vertical dashed lines mark the mean similarity score (−0.144) and the threshold for the top 30 candidate herbs (−0.044). e: Two-

dimensional visualization in the latent space of the Autoencoder. AE Dimension 1 captures the primary variation in transcriptomic data; AE Dimension 2 captures secondary variation. Points are colored by sample type: gray for other herbs, reddish-brown for top 30 candidate herbs, and dark blue for the positive control drug. Point size corresponds to cosine similarity with the positive control (larger points indicate higher similarity). f: Top 30 herbs identified by Autoencoder-based similarity analysis. g: Kernel weight distribution in the Multiple Kernel Learning (MKL) model. Radial basis function kernel (rbfdot, weight 0.5) captures nonlinear relationships; linear kernel (vanilladot, weight 0.5) identifies linear correlation patterns in gene expression. h: Distribution of MKL-based similarity scores between Chinese herbs and the positive control. The x-axis represents similarity scores; the y-axis shows counts. Most scores fall between 0 and 100 (peak ~50), with a long tail up to 400. i: Top 30 candidate herbs selected by Multiple Kernel Learning.

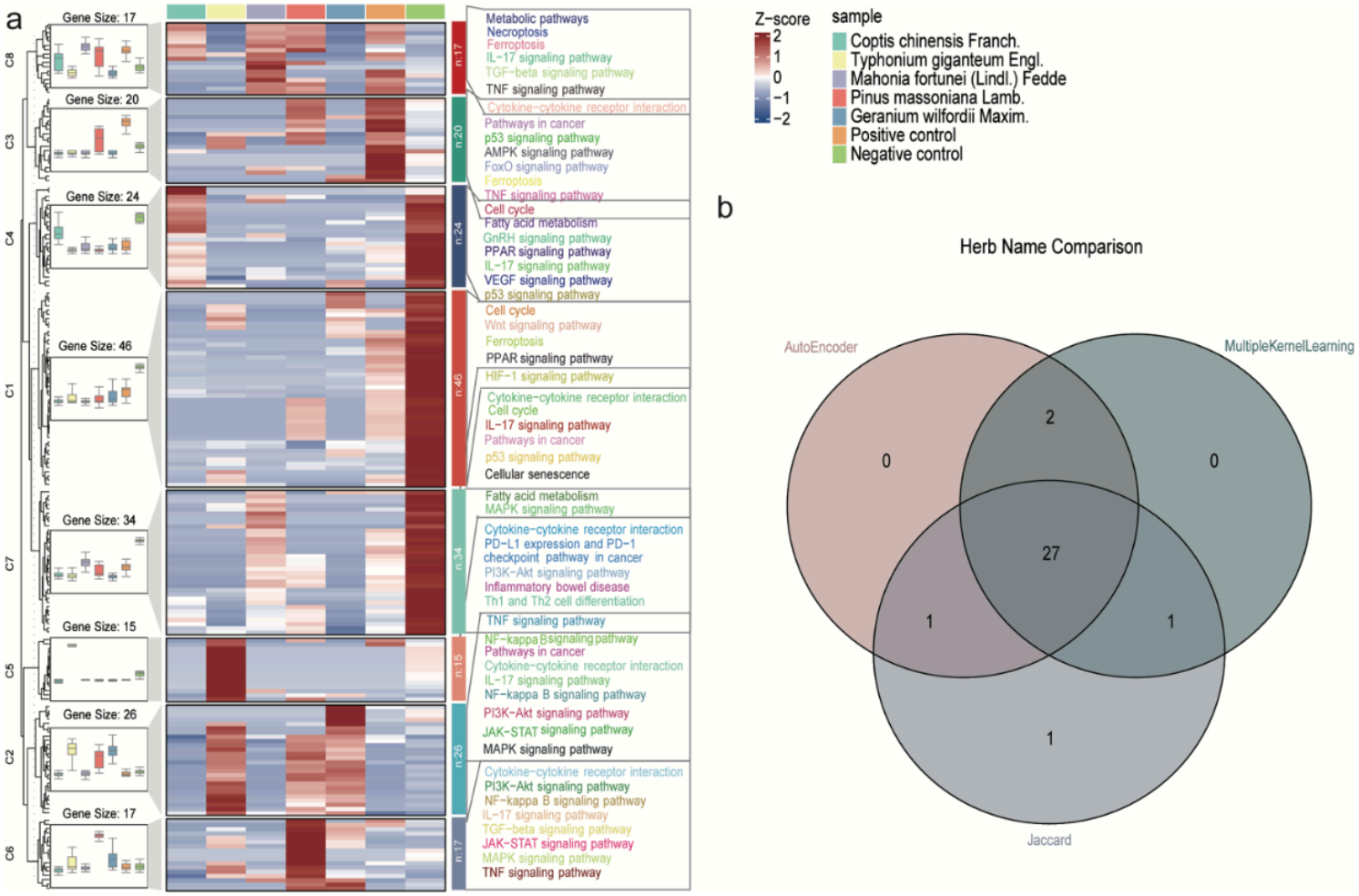

Figure 2

a: illustrates the changes in gene expression within the core pathway following different fraction treatments. The line chart on the left displays a clustering of all core genes, with eight clusters identified based on the inflection point. Additionally, a diagram categorizing gene expression and function within the pathways associated with the fraction experimental group, blank control group, and positive control group is provided. The violin plot on the left represents the proportion of gene expression for each component within the cluster. The intermediate heatmap depicts the changes in gene expression for each component, while the right side offers commentary on the cluster functions. b: utilized a combination of Jaccard index and deep learning model training to compare the top 30 medicinal plants with the positive control anti-cancer mechanism, revealing that 27 plants were shared between them(29–32).

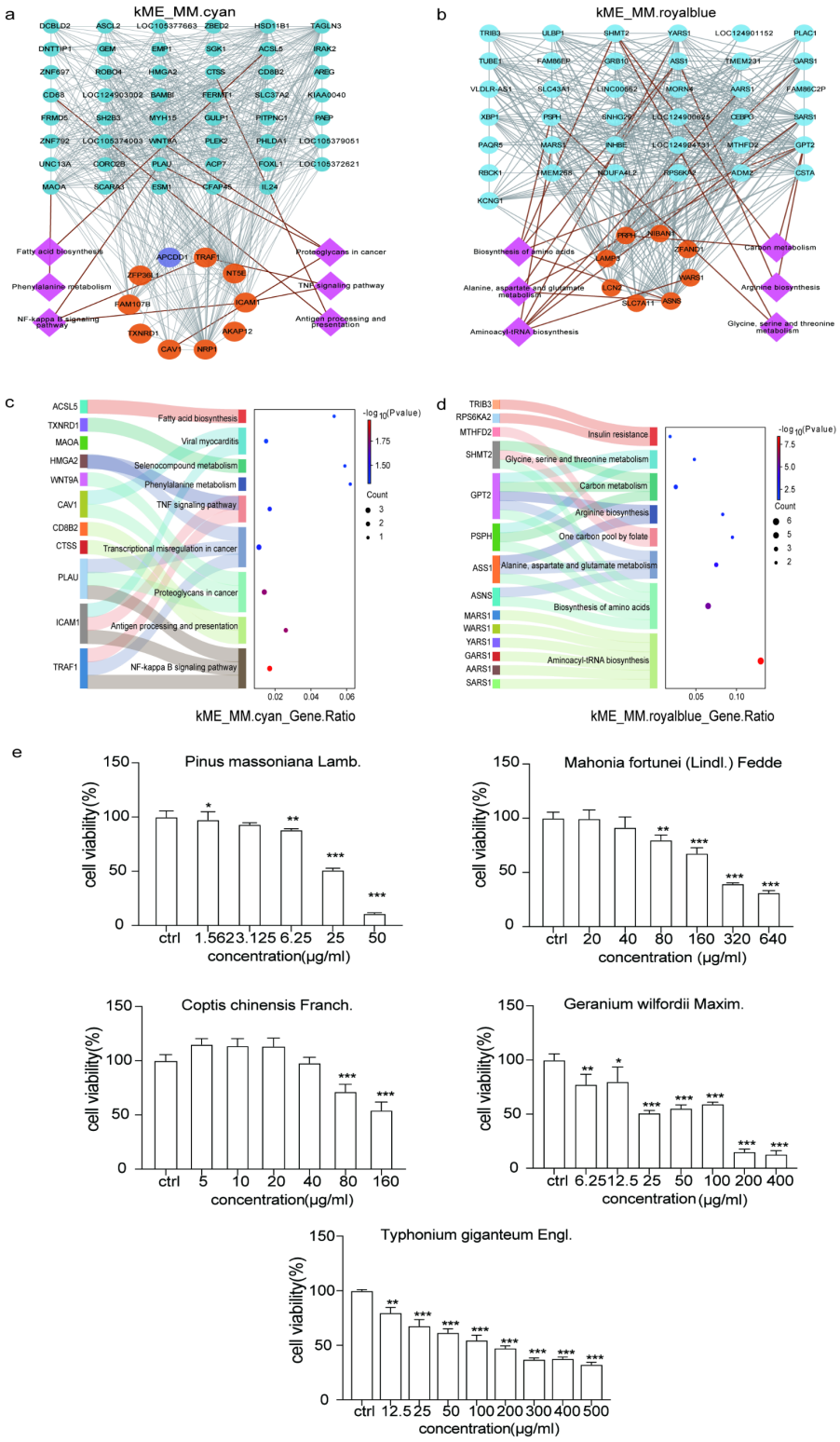

Figure 3

a-b depicts the network diagram of the core genes within the key module, where the dots represent genes that meet the criteria of degree ≥ 20 and weight ≥ 0.1. In this diagram, circles denote core genes, with orange representing upregulated genes and purple indicating downregulated genes. The pathways connected to the core genes are shown by the pink square nodes. c-d displays the Sankey bubble chart displaying the KEGG analysis of the core module. The gene ratio is displayed on the X-axis, and pathway names are provided on the Y-axis. Dot size indicates the count value, and dot color indicates the P-value. Genes linked to pathways are shown in the Sankey diagram on the left, with lines showing their connections.e:The

results of MTT experiments carried out at various gradient concentrations for each fraction group are depicted in the figure. The X-axis shows the dosage gradient concentration, and the Y-axis represents cell survival. *** p ≤ 0.001, ** p ≤ 0.01, and * p ≤ 0.05. KEGG pathway map reproduced with permission from Kanehisa Laboratories(29–32).

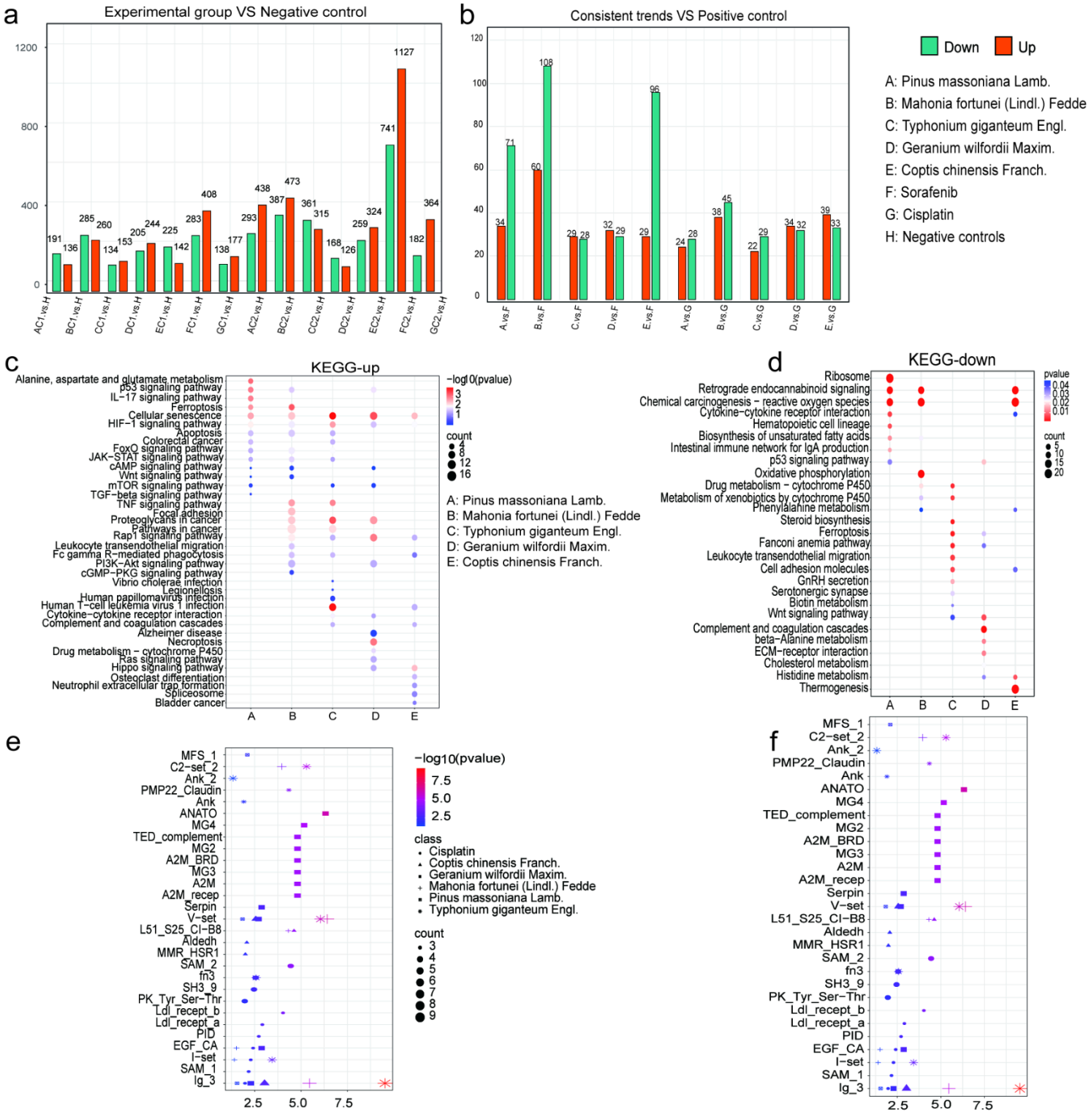

Figure 4

Proteome Differential Analysis. a: displays the number of upregulated and downregulated proteins compared to the negative control within each group, with the X-axis representing the comparison groups and the Y-axis indicating the quantity of differential proteins. b: shows a trend in line with the positive control group by statistically analyzing the differential proteins

for each distillation group. c-d: illustrate the KEGG pathways enriching the main components, with the X-axis representing the distillation groups and the Y-axis signifying the respective terms. The size and color of the bubbles in these figures correspond to count values and p-values, respectively. e-f: present the PFAM enrichment analysis for upregulated proteins, aligning with the expression trends observed in both experimental and positive control groups. In these graphics, enrichment is represented by the X-axis, and words are shown on the Y-axis. Different shapes stand in for different experimental groups; p-values are shown by the color intensity and count values are indicated by the size of the shapes. The KEGG pathway map is reprinted with permission from Kanehisa Laboratories(29–32).

Supplementary Files

This is a list of supplementary files associated with this preprint. Click to download.

- Table1.xlsx
- Table2.xlsx
- SupplementaryFiles.zip
- KEGGPERMISSION252104.pdf